

RSC Advances



This is an *Accepted Manuscript*, which has been through the Royal Society of Chemistry peer review process and has been accepted for publication.

Accepted Manuscripts are published online shortly after acceptance, before technical editing, formatting and proof reading. Using this free service, authors can make their results available to the community, in citable form, before we publish the edited article. This *Accepted Manuscript* will be replaced by the edited, formatted and paginated article as soon as this is available.

You can find more information about *Accepted Manuscripts* in the [Information for Authors](#).

Please note that technical editing may introduce minor changes to the text and/or graphics, which may alter content. The journal's standard [Terms & Conditions](#) and the [Ethical guidelines](#) still apply. In no event shall the Royal Society of Chemistry be held responsible for any errors or omissions in this *Accepted Manuscript* or any consequences arising from the use of any information it contains.

ARTICLE

Self-polarization induced by lattice mismatch and defect dipole alignment in (001) BaTiO₃/LaNiO₃ polycrystalline film prepared by magnetron sputtering at low temperature

Cite this: DOI: 10.1039/x0xx00000x

Y.F. Hou^a, T.D. Zhang^a, W.L. Li^{*ab}, W.P. Cao^a, Y. Yu^a, D. Xu^a, W. Wang^a, X.L. Liu^c and W.D. Fei^{*a}Received 00th January 2012,
Accepted 00th January 2012

DOI: 10.1039/x0xx00000x

www.rsc.org/

Upward self-polarization phenomenon was observed and studied in the highly (001)-oriented BaTiO₃/LaNiO₃ polycrystalline film, and the polycrystalline film was in situ prepared by radio frequency magnetron sputtering at 400°C without post treatment. The low temperature crystallization and high orientation of BaTiO₃ polycrystalline film may be caused by the better compatibility between BaTiO₃ and LaNiO₃. The upward self-polarization phenomena was characterized by piezoelectric force microscopy (PFM), and the coupling effects of low crystallization temperature, high (001) orientation, large compressive strain gradient and preferred orientation of defect dipoles are considered to be responsible for the upward self-polarization phenomena in the BaTiO₃/LaNiO₃ polycrystalline film during the cooling process, especially when ferroelectric domains nucleate and grow near 120°C.

1. Introduction

In most cases, the spontaneous polarization domains in as-prepared ferroelectric thin films are randomly orientated, and the macroscopic polarization appears under an external electric field (E_{ex}) larger than their coercive field (E_{C})¹. The macroscopic polarization will disappear for a short period of time due to the depolarization effect after E_{ex} is removed², thus it is very difficult to use the built-in electric field (E_{in}) derived from the macroscopic polarization. In addition, the films in the related devices without electrodes cannot be polarized. Furthermore, it is rather difficult to polarize the ferroelectric film with large coercive field or low-resistance at room temperature by an external electric field³. To overcome these difficulties, researchers have studied the self-polarization (macroscopic polarization without external electric field) in ferroelectric films under special conditions^{4, 5}. The self-polarization films provide an opportunity to design some novel devices based on the built-in electric field (E_{in}) generated by the self-polarization. Generally, the self-polarization films can only be grown by using epitaxial technology or crystallized at a high temperature (>500°C). While, the nature of the macroscopic self-polarization remains a subject of much controversy⁶, although various mechanisms related to the action of both electric fields and mechanical forces have been proposed in the ferroelectric thin film^{3, 4, 7, 8}. In addition, it is also a challenge to prepare self-polarization polycrystalline ferroelectric films at lower processing temperature to be compatible with the integrated technology of silicon (<450°C).

BaTiO₃ (BT) ceramics and films have been widely investigated because of the simple chemical composition and remarkable properties of BT⁹⁻¹². However, high-temperature annealing ($\geq 700^\circ\text{C}$) is regularly required to crystallize the pure BT

ferroelectric thin films. Recently, Ouyang *et al*¹³ have reported BT thin film can be crystallized at 500°C by a radio frequency magnetron sputtering (RF-MS) under a suitable proportion of Ar/O₂. Besides, it has been found that the crystallization temperature of ferroelectric films can be reduced by using buffer layer, because the crystallization nucleation of ferroelectric films is much easier on buffer layer than that on the Si or Pt substrate¹⁴⁻¹⁷. In addition, buffer layers have been also widely employed to prepare highly-oriented polycrystalline films¹⁸⁻²⁰. For example, Qiao *et al*²¹ have reported (001)-oriented BT films can be induced by LaNiO₃ (LNO) buffer layer. Moreover, a large compressive or tensile strain gradient can be induced by the lattice mismatch between the ferroelectric films and buffer layer or substrate, which is very important for the self-polarization films²²⁻²⁴.

Taking all the above into consideration, in order to prepare self-polarization BT polycrystalline film at low temperature, 3:1 Ar/O₂ flow ratio and LNO buffer layer are used in this study. In the present study, we report a simple in situ method to obtain self-polarization polycrystalline BT/LNO ferroelectric film with high (001) orientation by radio frequency magnetron sputtering (RF-MS) at 400°C without post treatment. For comparison, BT polycrystalline film without LNO buffer layer, which was crystallized at 750°C, was also prepared via the same method. In addition, the effects of LNO buffer layer and the self-polarization mechanism of BT film were discussed.

2. Experimental

The LNO buffer layer was introduced on the Pt/Ti/SiO₂/Si substrate using a sol-gel technique before the growth of BT film, as reported previously²⁵. A base pressure of 5.0×10^{-4} Pa was achieved in the deposition chamber prior to the deposition. The BT films deposition on the Pt/Ti/SiO₂/Si substrate with and without LNO

buffer layer were carried out at a substrate temperature of 400°C with the RF power of 40W for 2 hours, under a 3:1 Ar/O₂ flow ratio. After deposition, the films were cooled to room temperature in vacuum chamber. It is found that the as-prepared BT film without LNO buffer layer is amorphous, so the as-prepared BT film without LNO was crystallized at 750°C for 30 min in air. The top platinum electrodes with a size of 3.14×10^{-4} cm² were deposited by the DC magnetron sputtering, and the top platinum electrodes were used in the electric properties testing.

X-ray diffraction (XRD) characterizations of the BT thin films were performed using Cu K α radiation on an X'pert diffractometer. Surface and cross-sectional morphologies of BT thin films were observed by scanning electron microscopy (Helios Nanolab600i). The leakage current behaviours and *P-E* hysteresis loops of the samples were measured using a Radiant Precision Workstation Ferroelectric Measurement System. The frequency dependence of the dielectric permittivity and dielectric loss of the BT thin films were characterized by the Agilent 4294A precision impedance analyzer at the frequencies ranging from 500 Hz to 1 MHz. The surface morphologies and domain imaging of the films were obtained by the modified commercial atomic force microscope (AFM) with a piezoelectric force microscope (PFM) mode (Bruker multimode 8). The piezoelectric response signals from vertical cantilever deflection (proportional to the out-of-plane polarization) was acquired using the Conductive Pt-Ti-coated silicon cantilevers in the polarization switching studies.

3. Results and discussion

Fig. 1(a) shows θ - 2θ scan XRD patterns of BT films with and without LNO buffer layer on Pt/Ti/SiO₂/Si substrates. According to our previous report²⁶, the thickness of LNO is ~ 10 nm, and there is no diffraction peak of LNO in the corresponding XRD. It can be seen that the BT film without LNO buffer layer is amorphous at 400°C deposition temperature (BT-400 curve in Fig. 1a), and it can be crystallized after treatment at 750°C for 30 min (BT-750 curve in Fig. 1a). Meanwhile, no obvious preferential orientation can be found in the crystallized BT film without buffer layer. However, the BT film with LNO buffer layer is well crystallized at 400°C during deposition process (BT/LNO-400 curve in Fig. 1a), and there is no detectable secondary phase besides the tetragonal perovskite structure of BT.

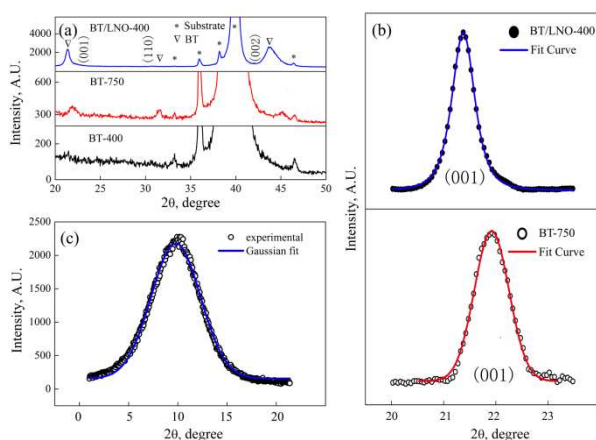


Fig. 1 θ - 2θ scan XRD patterns (a) of BT-400, BT-750 and BT/LNO-400 film, the measured and fitted profiles of (001) peaks (b) for BT/LNO-400 and BT-750, and ω scan XRD (rocking curve) patterns (c) for the (001) reflection of BT/LNO-400.

According to the PCPDF data (#83-1880) and comparison result given in Fig. 1(b) of fine XRD scan curves, only (001) peak

can be observed in both BT-750 and BT/LNO-400 film. The (001) diffraction angle for BT/LNO-400 film is greatly shifted to the lower angle suggesting the existence of large compressive strain of BT in the BT/LNO-400 film, while the (001) diffraction angle for BT-750 film is close to that of the PCPDF data (#83-1880) indicating the weak compressive strain of BT in the BT-750 film. In addition, only the (001) and (002) peaks can be clearly found in BT/LNO-400 film as shown in Fig. 1(a), which suggests that BT/LNO-400 film is highly (001)-oriented. To further evaluate the misorientation degree of BT/LNO-400 film^{27,28}, XRD rocking curve of BT/LNO-400 thin film was measured for the (001) reflection as shown in Fig. 1 (c). The rocking curve can be fitted by Gaussian function, and the Gaussian width (FWHM) for the film is about 5.9 degrees, which further indicates that the film obtained in the present study is highly (001)-oriented.

The above results indicate that the LNO buffer layer is very benefit to the crystallization of BT films, which leads to in situ crystallization of BT films during the RF-MS process even at the low temperature of 400°C. BT preferential nucleation on the LNO surface is the reason for such low temperature crystallization and high orientation of BT/LNO thin film, which is consistent with previous reports^{15,20}.

Fig. 2(a) and (b) show the surface micrographs of BT/LNO-400 and BT-750 thin films, respectively, it can be seen that the films exhibit dense, cracks free and uniform microstructures. The cross-section micrographs of BT/LNO-400 and BT-750 thin films are shown in Fig. 2(c) and (d), respectively. The cross-section micrographs show that there are some columnar structures in the BT/LNO-400 film, while some equiaxed grains rather than columnar grains are existed in the BT-750 film. Besides, it can be also seen from the cross-section micrographs that the thickness of BT/LNO-400 and BT-750 thin films is 180 nm and 245 nm, respectively. Thus, both BT/LNO-400 and BT-750 thin films have a densely packed microstructure at the microscopic scale. In addition, both the grain size and thickness of BT/LNO-400 thin film are much smaller than that of BT-750 thin film due to the lower crystallization temperature.

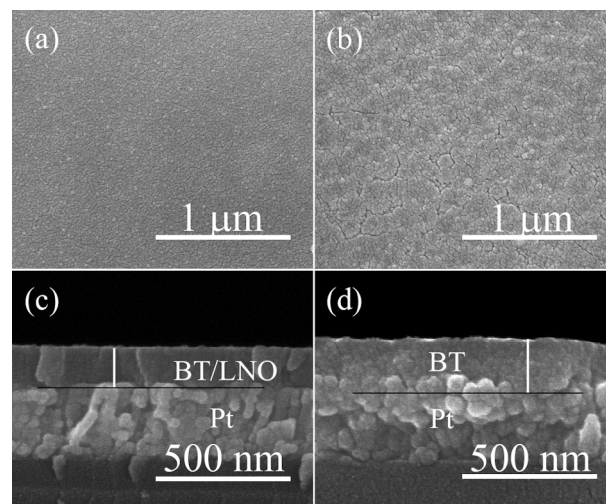


Fig. 2 Surface and cross-sectional micro-graphologies of BT films, (a) and (c) BT/LNO-400, (b) and (d) BT-750

To estimate the residual stress gradient in the BT/LNO-400 thin film, grazing incidence X-Ray diffraction^{29,30} (GIXD) method was used, where, 2θ is changed continuously with the fixed grazing incidence angle (ω). The schematic of GIXD measurement is shown in Fig. 3(a), where $\mathbf{K} = \mathbf{k} - \mathbf{k}_0$, \mathbf{K} , \mathbf{k}_0 and \mathbf{k} represent the scattering vector, incident wave vector and scattering wave vector,

respectively. The GIXD peaks of the (001) planes, obtained with the values of ω gradually increased from 3° to 10° along the direction of the arrow, for BT/LNO-400 thin film are shown in Fig. 3(b). It is clear that the increasing of incident angle (ω) is corresponding to the increasing of the penetration depth of X-ray. Therefore, the strain distribution behaviour along z direction (the normal direction of films) in the film can be revealed by GIXD method with different ω values.

It is clear that the stresses and strains of the films can be assumed as axisymmetric ones. In the coordinate system shown in Fig. 3(a), we have $\varepsilon_x = \varepsilon_y \equiv \varepsilon_{xy} \neq \varepsilon_z$, $\sigma_z = 0$, $\sigma_x = \sigma_y$, where ε_x , ε_y , ε_z are the normal strains, and σ_x , σ_y , σ_z are the normal stresses. In the axisymmetric model, according to the Hooke's law, we have

$$\varepsilon_x = \frac{\sigma_x}{E} - \frac{\nu}{E}(\sigma_y + \sigma_z) = -\frac{1-\nu}{E}\sigma_x \quad (1)$$

$$\varepsilon_z = -\frac{\nu}{E}(\sigma_x + \sigma_y) = -\frac{2\nu}{1-\nu}\varepsilon_x = -\frac{2\nu}{1-\nu}\varepsilon_{xy} \quad (2)$$

where, ν is the Poisson ratio of BT ceramic, and $\lambda = 2\nu/(1-\nu)$.

The normal strain (ε_K) along K direction is

$$\varepsilon_K = \sin^2\psi\varepsilon_{xy} + \cos^2\psi\varepsilon_z \quad (3)$$

where, $\psi = \theta - \omega$, which can be derived from Bragg's equation and geometric relation given in Fig. 3(a), and $\varepsilon_K = (d_K - d_0)/d_0$ (where d_K is the interplane spacing along K direction, d_0 is the interplane spacing of stress free specimen). ε_K depends on the distance from the film surface when the stress in the film is inhomogeneous along z direction, and can be measured by the GIXD with different incident angles. In the right side of equation (3), the first term can be ignored because $\sin^2\psi$ is much smaller than $\cos^2\psi$ ($\psi = \theta - \omega < 8^\circ$) in our experiment. Taking equation (1)-(3) into consideration, the equation (4) can be obtained

$$\frac{\varepsilon_K}{\cos^2\psi} = \varepsilon_z = -\lambda\varepsilon_{xy} \quad (4)$$

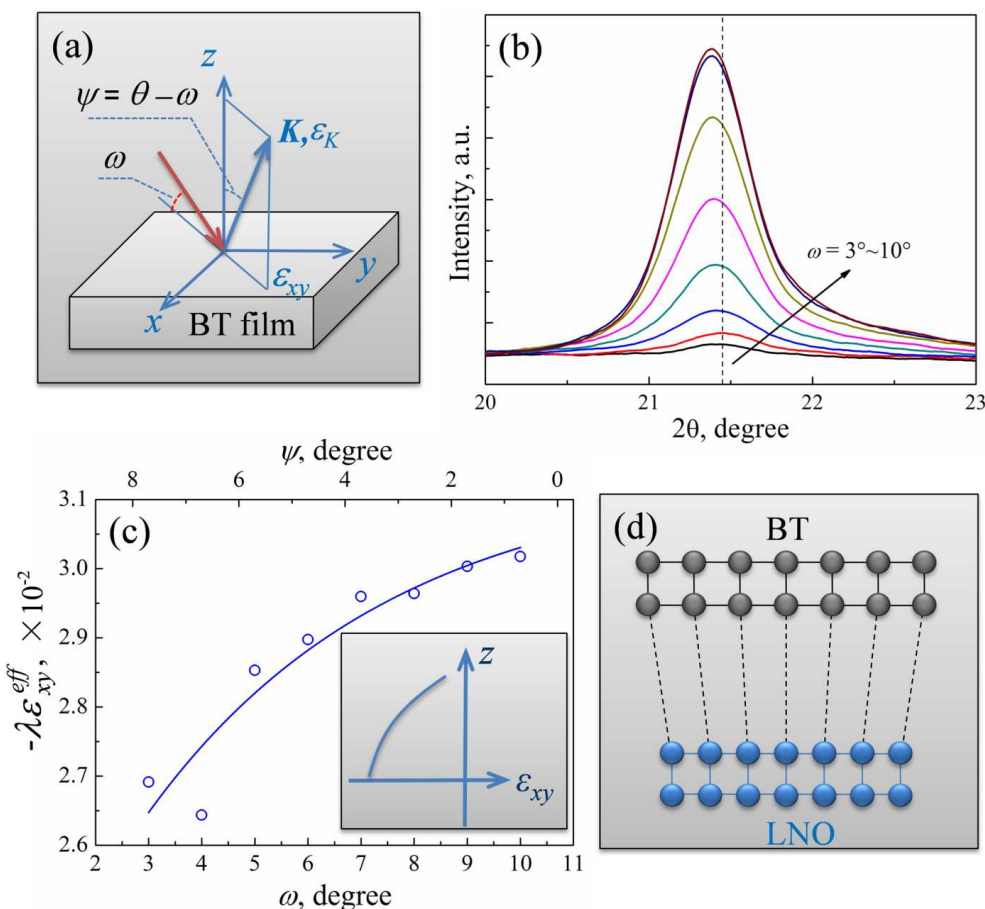


Fig. 3 (a) Schematic of GIXD measurement, (b) GIXD of (001) of BT/LNO-400 with ω range from 3° to 10° along the direction of the arrow, (c) $-\lambda\varepsilon_{xy}^{eff}$ against ω and ψ of BT/LNO-400, where the solid line is the fitted result by exponential function, inset is z against ε_{xy} , where $z = 0$ represents the interface between BT and LNO, (d) schematic of BT and LNO lattice mismatch

from the interface between BT ($a=0.3994$ nm and $c=0.4038$ nm)³ and LNO (0.3840 nm)³¹, as shown in the inset figure of Fig. 3(c). In other words, lattice parameter of BT in the top is larger than that in the bottom due to the lattice mismatch between BT and LNO, as shown in Fig. 3(d). Therefore, there is a compressive stress gradient between the two surfaces of BT film.

According to the Bragg's equation $2d\sin\theta = \lambda$ and the diffraction results from Fig. 3(a). The strain measured at different incident angles, denoted as ε_{xy}^{eff} , is the average value of the strain in the X-ray penetration depth, and not the true value of ε_K corresponding to a certain depth. But there exists a positive relation between ε_K^{eff} and ε_K . Therefore, $-\lambda\varepsilon_{xy}^{eff}$ derived from ε_K^{eff} and Equation (4), can reflect the changing tendency of $-\lambda\varepsilon_{xy}$. $-\lambda\varepsilon_{xy}^{eff}$ for (001) reflection against ω and ψ is shown in Fig. 3(c). From Fig. 3(c), it can be observed that the $-\lambda\varepsilon_{xy}^{eff}$ value increases with ω increasing, which means that compressive strain ε_{xy} decreases with z increasing

It is difficult to determine the domain orientation in BT/LNO-400 film using XRD technique although the high (001) orientation is confirmed by both θ - 2θ and ω scan XRD analysis. To investigate the domain orientation of highly (001)-oriented BT/LNO-400 film,

the PFM image analysis was performed. The AFM and PFM images were taken after poling the adjacent area with positive and negative voltages, where both poled and unpoled regions of the film were imaged simultaneously. The surface morphologies (AFM mode) of BT/LNO-400 and BT-750 do not exhibit a significant change before and after polarization with a DC bias voltage of 5V, and the surface roughness of BT-750 is much larger than that of BT/LNO-400, as shown in Fig. 4(a) and (b).

To obtain the domain structure using PFM, the voltage was applied between the bottom electrode and PFM tip, and the tip was grounded. The positive piezoelectric response signal implies upward polarization because the sign of the piezoelectric signal is proportional to the out-of-plane polarization. Thus the bright domains correspond to upward polarization, and dark domains result from the downward or in-plane polarization. The representative out-of-plane PFM images recorded on unpoled and poled BT/LNO-400 film are shown in Fig. 4(c), it can be seen that the unpoled BT/LNO-400 film (0V) is consists of nanodomains with almost upward polarization (the left region in Fig. 4c). In the positively poled state (5V), the nanodomains are upward polarized (the right region in Fig. 4c), and the PFM image of the positively poled film is very similar to that of the as-grown film. The above observations suggest the BT/LNO-400 thin film exhibits upward self-polarization feature.

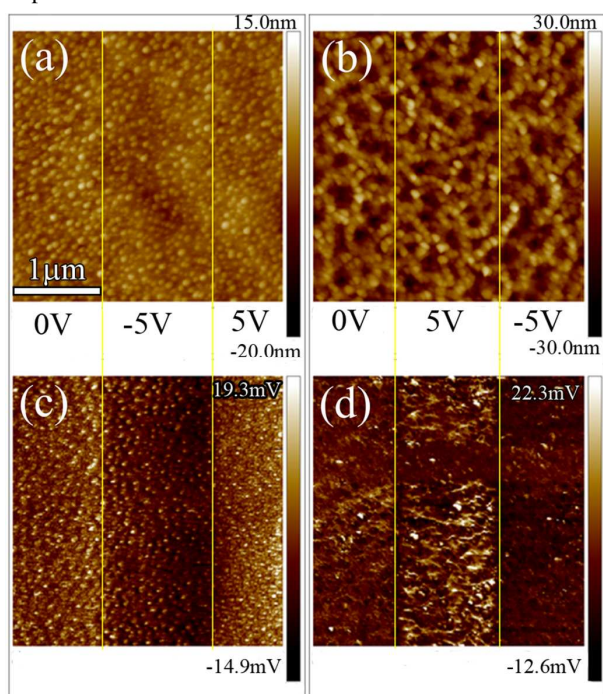


Fig. 4 AFM surface morphologies of BT/LNO-400 film (a) and BT-750 film (b), and PFM domain structures of BT/LNO-400 film (c) and BT-750 film (d). The surface morphologies (a, b) and domain structures (c, d) were simultaneously captured under different bias (the left region (0V) corresponding to the unpoled state, the middle and right region (-5V and 5V) corresponding to poled region)

During the observation of negatively poled state (-5V) of BT/LNO-400 film, it is found that the nanodomains are almost composed of downward polarization during the negative voltage applying. However, downward domains gradually switch spontaneously to upward ones when the negative voltage is removed. Therefore, the brightness of PFM image of negatively poled region (see the middle region in Fig. 4c), taken after negative voltage removing, decreases from left to right, and the brighter

region of the middle image in Fig. 4(c) is corresponding to early negative polarization (where it should be negative polarization before negative bias removing). The results indicate that the upper self-polarization in the BT/LNO-400 thin film is quite stable, which is very important for the applications of the self-polarization films.

While for the BT-750 film the nanodomains are composed of both upward and downward polarization in the as-grown state (the left region in Fig. 4d), which is different from either the positively poled state (the middle region in Fig. 4d) or the negatively poled state (the right region in Fig. 4d). Thus the self-polarization is nonexistent in the BT-750 film.

The dielectric properties of BT/LNO-400 and BT-750 films are shown in Fig. 5(a) at room temperature, as a function of measuring frequency ranging from 500 Hz to 1 MHz.

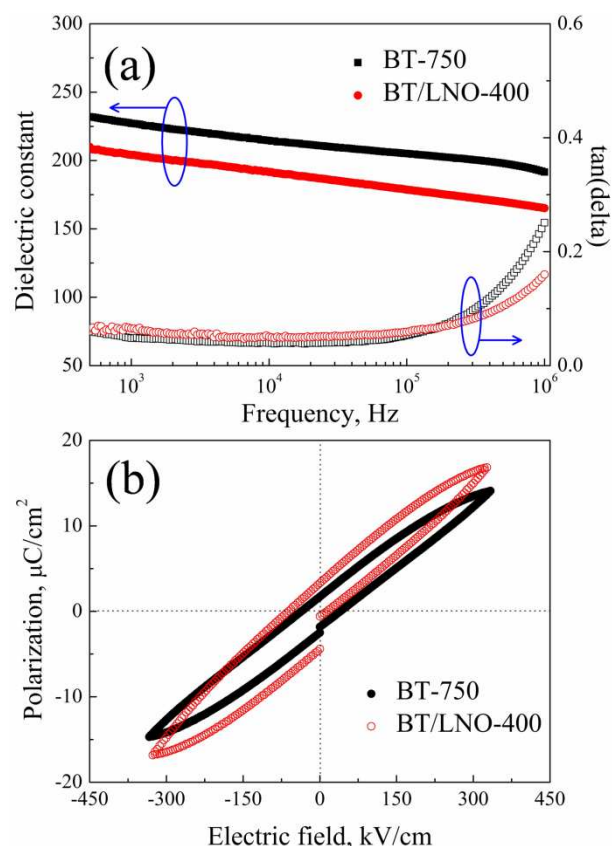


Fig. 5 Electric properties of BT-750 and BT/LNO-400 polycrystalline films, (a) frequency dependence of dielectric permittivity and dielectric loss (b) P - E hysteresis loops.

From Fig. 5(a), it can be observed that the dielectric constants of BT/LNO-400 and BT-750 films are 200 and 220 at the frequency of 1 kHz, respectively. The dielectric losses of both BT/LNO-400 and BT-750 films show little frequency dispersions at lower frequencies and strong frequency dispersions at higher frequencies. The strong frequency dispersions at higher frequencies are caused by the dielectric relaxation, which is typical of the ferroelectric thin films^{32,33}.

Fig. 5(b) shows the ferroelectric polarization versus electric field curves (P - E hysteresis loops) of the BT/LNO-400 and BT-750 films measured at 1 kHz. The unclosed and slanted P - E loop of BT/LNO-400 thin film is caused by the increasing leakage current³⁴ and nonuniformity of the domains³⁵. And both the increasing leakage current and nonuniformity of the domains are caused by the low density of aligned defect dipoles in the BT/LNO-400 film during the preparation process, which will discuss later.

The positive (E_C) and negative (E_C') coercive electric fields should be close to each other in symmetric P - E loops. In the BT-750 thin film, $E_C = E_C' \approx 38$ kV/cm, however, in the BT/LNO-400 thin film, E_C is 13 kV/cm and E_C' is -63 kV/cm as shown in Fig. 5(b). The discrepancy between E_C and E_C' in the BT/LNO-400 thin film is derived from the upward self-polarization⁴. A more negative bias is needed because the ferroelectric polarization induced by the negative bias counteracts the upward self-polarization³⁶.

To further confirm the self-polarization phenomena and the accompanied built-in electric field in the BT/LNO-400 film, I-V curves were characterized and shown in Fig. 6.

As shown in Fig. 6, very similar conductive behaviours are observed in the BT-750 film under both positive and negative bias voltage. While the BT/LNO-400 film exhibits unidirectional conductive characteristic, namely it is conductive under positive bias, and it is not conductive under negative bias. This discrepancy of conductive behaviour between BT-750 and BT/LNO-400 films is attributed to the built-in electric field in the BT/LNO-400 thin film³⁷, which is caused by the self-polarization effect. The results of I-V curves of BT/LNO-400 thin film further confirm the existence of a stable built-in electric field in the self-polarization thin film. Hence, the BT/LNO thin film can provide a constant electric field for other devices due to its stable built-in electric field caused by the upward self-polarization.

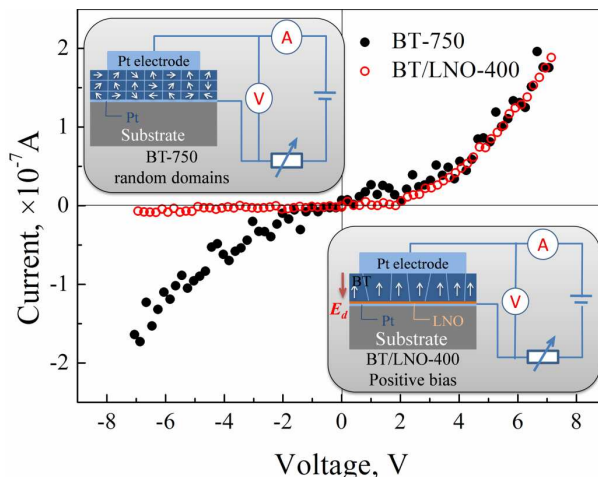


Fig. 6 The leakage current behaviour of BT-750 and BT/LNO-400, insert is the schematic of I-V measurement of BT-750 and BT/LNO-400.

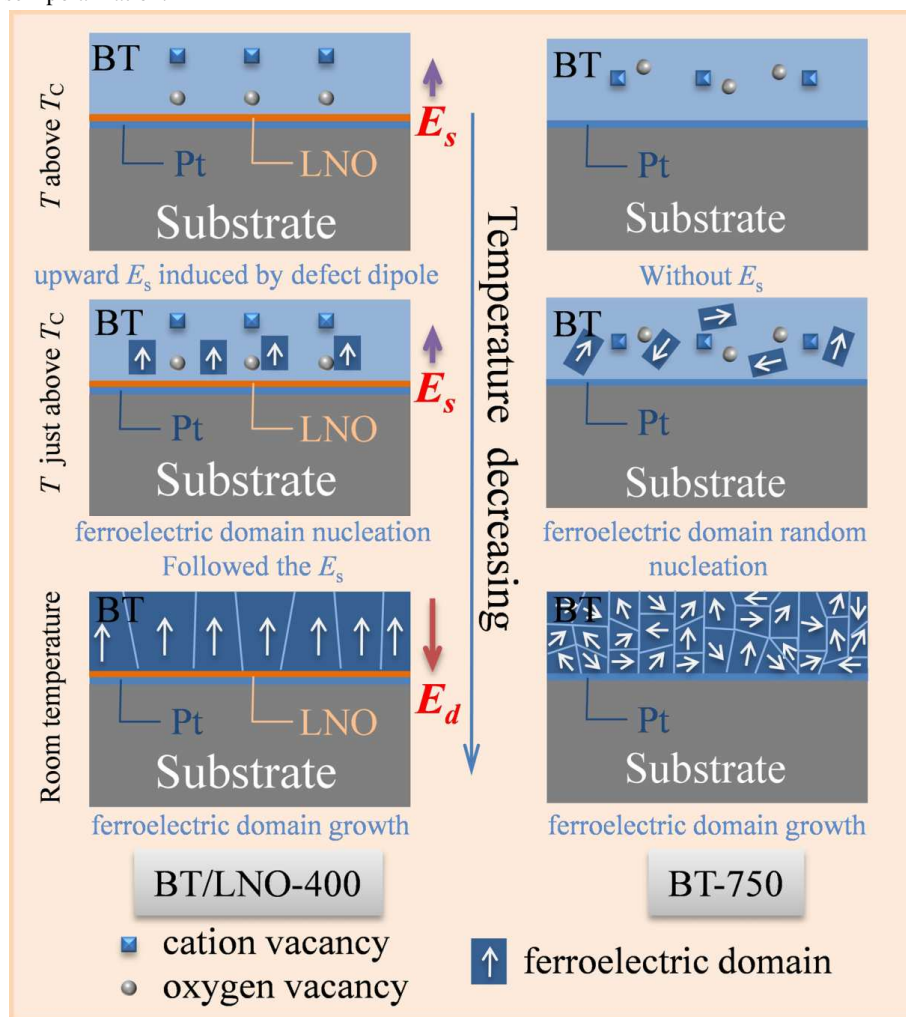


Fig. 7 The forming process of self-polarization of BT/LNO-400 and BT-750 film

The large compressive stress gradient is determined in BT/LNO-400 film as shown in Fig. 3, which is one of the most

possible reasons for the upward self-polarization in the BT/LNO-400 thin film^{3, 8, 36}. Besides, both low crystallization temperature

and high (001) orientation of BT/LNO-400 thin film are also critical to the upward self-polarization. In the sputtering process, oxygen vacancies are inevitably introduced to the BT/LNO-400 thin film in lower oxygen pressure. Besides, cation (Ba^{2+} or Ti^{4+}) vacancies may also exist in the non-stoichiometric BT. Vacancies in the film should diffuse to BT/LNO interface in order to relax the elastic energy caused by the large compressive strain gradient in the BT/LNO-400 film^{38, 39}. Because the diffusion coefficient of oxygen vacancy is much larger than those of cation vacancies in titanate materials⁴⁰, the oxygen vacancy diffusion to BT/LNO interface in the film is dominant. At the same time, the cation vacancies may stay in-situ for the stability of the BT cell lattice. Thus, a mass of defect dipoles with an upward E_s (the E_s is defined as the electric field generated by the separated oxygen and cation vacancies) are formed by the separated the oxygen vacancies and cation vacancies, as shown in Fig. 7. When the temperature reaches T_C of BT on cooling, the nucleation and growth of upward ferroelectric domains are prior to other direction domains under the affection of the E_s , because the film is highly oriented. Furthermore, as the E_C of BT film at high temperature (close to T_C) is much smaller than that at room temperature, the upward E_s caused by aligned defect dipoles is possible to be larger than E_C . Thus, BT/LNO-400 film is possible to be poled by E_s at high temperature⁸. Finally, the upward self-polarization BT film is formed at room temperature. Correspondingly, a downward E_d (depolarization electric field) is also formed as shown in Fig. 7.

According to the discussion of Fig. 1(a), weak compressive strain gradient is existed in the BT-750 film. Besides, no preferred orientation is found in the BT-750 film. Thus, no preferred-oriented E_s is formed in the BT-750 thin film. With the temperature decreasing, the nucleation and growth of ferroelectric domains are randomly, as shown in Fig. 7. Finally, the ferroelectric domains are random orientation, and no self-polarization effect is observed in the BT-750 thin film.

4. Conclusions

In summary, upward self-polarization phenomena was observed and studied in the highly (001)-oriented BT/LNO-400 polycrystalline film. Using LNO as buffer layer, the BT polycrystalline film was in situ grown on a Pt/Ti/SiO₂/Si substrate via radio frequency magnetron sputtering at 400°C. The low temperature crystallization and high orientation of BT polycrystalline film may be caused by the better compatibility between BT and LNO. The coupling effects of low crystallization temperature, high (001) orientation, large compressive strain gradient and preferred orientation of defect dipoles are considered to be responsible for the upward self-polarization phenomena in the BT/LNO-400 polycrystalline film during the cooling process, especially when ferroelectric domains nucleate and grow near 120°C. The low temperature crystallization, high orientation and upward self-polarization of BT/LNO-400 polycrystalline film may provide a constant electric field for some Si-based devices where voltages or electrodes are forbidden.

Acknowledgements

The research was financially supported by the National Natural Science Foundation of China (No: 11272102) and Research Foundation of Shenzhen Science, Technology and Innovation Commission (No: ZDSY20120613125247154).

Notes and references

^a School of Materials Science and Engineering, Harbin Institute of Technology, Harbin 150001, People's Republic of China.

^b National Key Laboratory of Science and Technology on Precision Heat Processing of Metals, Harbin Institute of Technology, Harbin 150001, People's Republic of China

^c Department of Materials Science and Engineering, Harbin Institute of Technology Shenzhen Graduate School, Shenzhen 518055, P.R. China

* Corresponding authors: Electronic mail: wdfei@hit.edu.cn, wlli@hit.edu.cn

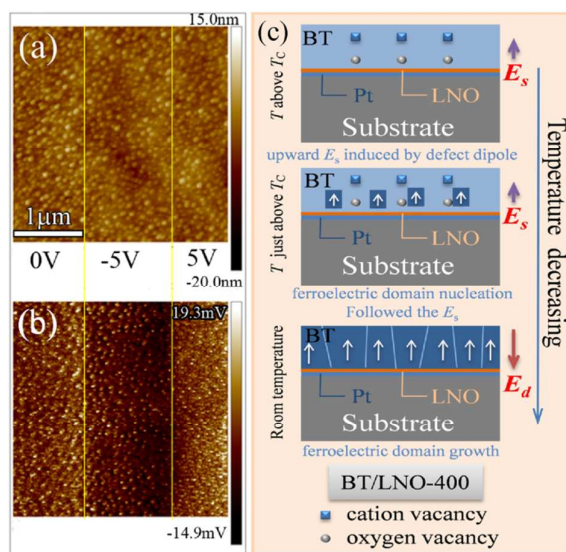
Fax/Tel: +86-451-86413908.

1. E. C. Lima, E. B. Araújo, I. K. Bdikin and A. L. Kholkin, *Materials Research Bulletin*, 2012, **47**, 3548-3551.
2. R. Bouregba, N. Sama, C. Soyer, G. Poullain and D. Remiens, *Journal of Applied Physics*, 2010, **107**, 232906.
3. J. Chen, Y. Luo, X. Ou, G. Yuan, Y. Wang, Y. Yang, J. Yin and Z. Liu, *Journal of Applied Physics*, 2013, **113**, 204105.
4. I. K. Bdikin, J. A. Pérez, I. Coondoo, A. M. R. Senos, P. Q. Mantas and A. L. Kholkin, *Journal of Applied Physics*, 2011, **110**, 052003.
5. I. Coondoo, N. Panwar, I. Bdikin, V. S. Puli, R. S. Katiyar and A. L. Kholkin, *Journal of Physics D: Applied Physics*, 2012, **45**, 055302.
6. V. P. Afanas'ev, I. P. Pronin and A. L. Kholkin, *Physics of the Solid State*, 2006, **48**, 1214-1218.
7. X. L. Zhao, B. B. Tian, B. L. Liu, J. L. Wang, L. Han, J. L. Sun, X. J. Meng and J. H. Chu, *Thin Solid Films*, 2014, **551**, 171-173.
8. X. Chen, Y. Zou, G. Yuan, M. Zeng, J. M. Liu, J. Yin, Z. Liu and X. M. Chen, *Journal of the American Ceramic Society*, 2013, **96**, 3788-3792.
9. J. B. Xu, J. W. Zhai and X. Yao, *Applied Physics Letters*, 2006, **89**, 202907.
10. M. Deluca, M. Higashino and G. Pezzotti, *Applied Physics Letters*, 2007, **91**, 071907.
11. A. Zenkevich, Y. Matveyev, K. Maksimova, R. Gaynutdinov, A. Tolstikhina and V. Fridkin, *Physical Review B*, 2014, **90**, 161409.
12. L. Wang, J. Wang, B. Li, X. Zhong, F. Wang, H. Song, Y. Zeng, D. Huang and Y. Zhou, *RSC Advances*, 2014, **4**, 21826.
13. M. Yuan, W. Zhang, X. Wang, W. Pan, L. Wang and J. Ouyang, *Applied Surface Science*, 2013, **270**, 319-323.
14. J.W. Moon, S. Tazawa, K. Shinozaki, N. Wakiya and N. Mizutani, *Applied Physics Letters*, 2006, **89**, 202907.
15. Q. G. Chi, W. L. Li, B. Feng, C. Q. Liu and W. D. Fei, *Scripta Materialia*, 2009, **60**, 218-220.
16. K. Fukamachi, N. Sakamoto, T. Ohno, D. Fu, N. Wakiya, T. Matsuda and H. Suzuki, *Japanese Journal of Applied Physics*, 2011, **50**, 09NA03.
17. L. Mazet, R. Bachelet, L. Louahadj, D. Albertini, B. Gautier, R. Cours, S. Schamm-Chardon, G. Saint-Girons and C. Dubourdieu, *Journal of Applied Physics*, 2014, **116**, 214102.
18. Y. Wang, Y. Lin and C.W. Nan, *Journal of Applied Physics*, 2008, **104**, 123912.
19. Q. G. Chi, X. Wang, W. L. Li, W. D. Fei and Q. Q. Lei, *Applied Physics Letters*, 2011, **98**, 242903.
20. Y.H. Lee, J.M. Wu, Y.L. Chueh and L.J. Chou, *Applied Physics Letters*, 2005, **87**, 172901.
21. L. Qiao and X. Bi, *Thin Solid Films*, 2009, **517**, 3784-3787.
22. A. Vailionis, W. Siemons and G. Koster, *Applied Physics Letters*, 2007, **91**, 071907.
23. D. Fuchs, E. Arac, C. Pinta, S. Schuppler, R. Schneider and H. v. Löhneysen, *Physical Review B*, 2008, **77**, 014434.
24. A. Vailionis, H. Boschker, W. Siemons, E. P. Houwman, D. H. A. Blank, G. Rijnders and G. Koster, *Physical Review B*, 2011, **83**, 064101.
25. T. D. Z. W. L. Li, Y. F. Hou, Y. Zhao, D. Xu, W. P. Cao and W. D. Fei, *RSC Advances*, 2014, **4**, 56933-56937.
26. W. L. Li, T. D. Zhang, D. Xu, Y. F. Hou, W. P. Cao and W. D. Fei, *Journal of the European Ceramic Society*, 2015, **35**, 2041-2049.
27. W. L. L. C. Q. Liu, W.D. Fei, S.Q. Zhang, J.N. Wang, *Journal of Alloys and Compounds*, 2010, **493**, 499-501.
28. W. D. F. S. Q. Zhang, W.L. Li, J.N. Wang, *Journal of Alloys and Compounds*, 2009, **487**, 703-707.
29. M. Marciszko, A. Baczański, M. Wróbel, W. Seiler, C. Braham, J. Donges, M. Śniechowski and K. Wierzbowski, *Thin Solid Films*, 2013, **530**, 81-84.
30. J. H. H. C.H. Ma, Haydn Chen, *Thin Solid Films*, 2002, **418**, 73-78.

Journal Name

31. S. Hussain, S. K. Hasanain, G. Hassnain Jaffari and S. Ismat Shah, *Current Applied Physics*, 2015, **15**, 194-200.
32. H. Huang, X. Yao, M. Wang and X. Wu, *Journal of Crystal Growth*, 2004, **263**, 406-411.
33. Y. Guo, K. Suzuki, K. Nishizawa, T. Miki and K. Kato, *Journal of Crystal Growth*, 2005, **284**, 190-196.
34. T.H. Zhang, Y.G. Liu, J.Q. Zhao, Z.H. Huang and M.H. Fang, *International Journal of Applied Ceramic Technology*, 2015, **12**, E134-E141.
35. H. W. Jang, D. Ortiz, S.H. Baek, C. M. Folkman, R. R. Das, P. Shafer, Y. Chen, C. T. Nelson, X. Pan, R. Ramesh and C.B. Eom, *Advanced materials*, 2009, **21**, 817-823.
36. Z. Wang, X. X. Zhang, X. Wang, W. Yue, J. Li, J. Miao and W. Zhu, *Advanced Functional Materials*, 2013, **23**, 124-132.
37. C. H. Jia, X. W. Sun, G. Q. Li, Y. H. Chen and W. F. Zhang, *Applied Physics Letters*, 2014, **104**, 043501.
38. R. a. Poyato, M. L. Calzada and L. Pardo, *Applied Physics Letters*, 2004, **84**, 4161.
39. G. L. Yuan, L. W. Martin, R. Ramesh and A. Uedono, *Applied Physics Letters*, 2009, **95**, 012904.
40. S. L. K. S. Y. Chung, *J. Am. Ceram. Soc.*, 2002, **85**, 2805-2810.

Table of contents entry



Upward self-polarization induced by lattice mismatch and defect dipole alignment in (001) BaTiO₃/LaNiO₃ polycrystalline film at low temperature.